Closed-loop control of weld penetration using front-face vision sensing

Y M Zhang*, PhD
National Laboratory for Welding, Harbin Institute of Technology, Harbin, China

R Kovacevic, PhD
Center of Robotics and Manufacturing Systems and Department of Mechanical Engineering, University of Kentucky, USA

L Wu, PhD
National Laboratory for Welding, Harbin Institute of Technology, Harbin, China

Feedback control of weld penetration based on a front-face sensor is a challenging problem in the field of welding. A novel vision-based approach is proposed in this paper for full penetration control of the gas tungsten arc welding (GTAW). Owing to the relationship between the front-face weld geometry and back-face weld width (representation of the full penetration state), which has been reported earlier by the present authors, it is possible to use the front-face geometry as feedback of full penetration. Based on the dynamic modelling and the analysis of accepted adaptive control algorithms, an adaptive predictive decoupling controller is developed. Simulations and experiments under a variety of welding conditions have been conducted to verify the effectiveness of the proposed approach and controller.

NOTATION

$\{a, y_0(a)\}$ and $\{b, y_0(b)\}$	coordinates of feature points
$\hat{a}$ and $\hat{b}$	estimated a and b
b	also used as front-face weld width, in short, the weld width
b_b	back-face weld width
b_{ij}	parameters of dynamic model
b_{j0}, λ_j	parameters of real-time model
d_0, d_1	parameters of l_1
d_{ij}	sub-delay of dynamic model
h	front-face average weld depression depth, in short, depression
i	welding current
$\bar{i}$, $\bar{l}$	generalized control variables
k	discrete time
k_0, k_1	parameters of straight-line approximation of c_2
l	arc length
l_1, c_2 and l_3	three segments of medial axis
M	sample size in straight-line fitting for feature points extraction
M_{ij}	sub-order of dynamic model
$pixel_x$ and $pixel_y$	resolutions of image sensor
T	sampling period
V	torch velocity
(x, y_0)	coordinates of medial axis
z_0	arc centre location
z_1	location of rear boundary of weld pool
z_2	location of widest part of weld pool
z_3	laser stripe location
ε_x	medial axis extraction error
θ	electrode tip angle

The MS was received on 11 August 1992 and was accepted for publication on 11 January 1993

* *Present Address: Center for Robotics and Manufacturing Systems, University of Kentucky, USA.*

1 INTRODUCTION

Researchers have conducted studies to find feasible approaches to the control of weld penetration, for either full penetration or partial penetration instances, utilizing front-face sensors. Much research has been based on the concept of using weld pool motion for pool geometry sensing (**1–7**). However, Hardt (**5**) and Sorensen (**4**) have shown that it is not practical to detect the pool shape in partial penetration, using the concept of pool oscillation through analysis and experiments. Also, it was demonstrated by Tam and Hardt (**6**) that, in the case of full penetration, the unique identification of the pool shape is unreliable if no other correlating data are available. The reflection ultrasound method was utilized to measure the size of the stationary weld pool by Hardt and Katz (**8**). Similarly, ultrasonic measurements of the weld pool were performed at the Idaho National Engineering Laboratory (**9–12**) and Brunel University (**13**). In a recent report, an effort to discriminate among different geometries of welds was presented (**12**). However, a more realistic non-contacting sensor-based system was under investigation (**12**). Studies have also been conducted in infrared sensing of welds (**14**, **15**). Recently, Chen and Chin utilized an infrared sensing technique to measure the welding temperature distribution (**15**). Relationships were obtained between the bead width as well as the depth of joint penetration with respect to the characteristics of the temperature profiles. However, although varying current was used to produce the variation in penetration, all other experimental parameters were held constant. It seems that variable experimental parameters should be addressed. In the United Kingdom, Liverpool University and Nuclear Electric plc have made contributions to this important problem.

The authors observed that a skilled human welder can obtain adequate information on the full penetration state by viewing the weld pool rear and the adjacent

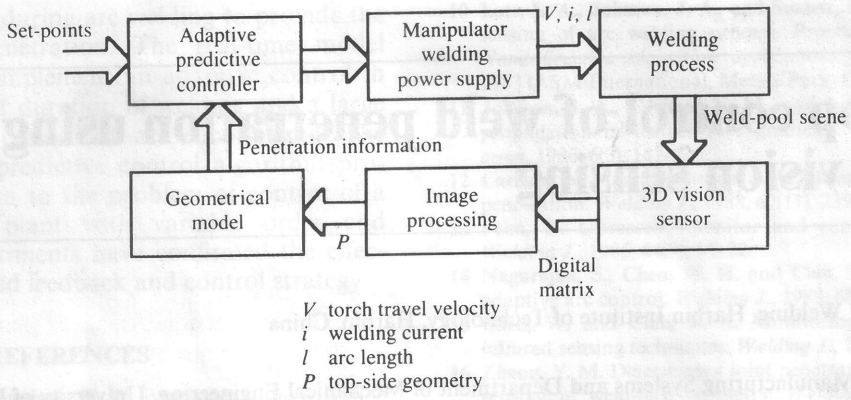

Fig. 1 Vision-based control of full penetration

solidified weld behind the pool. If the experience of the skilled human welder can be extracted, information on the full-penetration state can probably be obtained utilizing a machine vision approach. However, at present, sensing the three-dimensional geometry of the pool surface may be difficult. Thus, a full-penetration control strategy based on sensing the adjacent weld behind the pool is presented for the GTAW.

The proposed control principle is shown in Fig. 1. The weld penetration feedback is obtained through a geometric model, an image processing unit and three-dimensional vision sensor. The three-dimensional sensor acquires the images of the adjacent weld mentioned above, and the image-processing unit processes the images to calculate the front-face geometric parameters of the weld. The geometric model, which describes the relationship between the back-face weld width (which represents the full penetration state) and the front-face geometric parameters of the weld (**16**, **17**), then produces the final weld penetration feedback using the measured front-face geometrical parameters. Thus, these front-face geometrical parameters, the front-face weld width b and average weld depression depth h (see Fig. 2), must be measured as the feedback and controlled.

2 FEEDBACK MEASUREMENT

2.1 Sensing system

The principle of the three-dimensional vision sensing system is shown schematically in Fig. 3. In this sensing system, the structured-light plane is produced by means of a cylindrical lens. When this light plane is projected onto the adjacent weld behind the pool, a laser stripe forms. This laser stripe is perpendicular to the weld path. It can be seen that the laser stripe is the intersection of the weld zone and the light plane. Thus, the shape information of the cross-section of the weld has

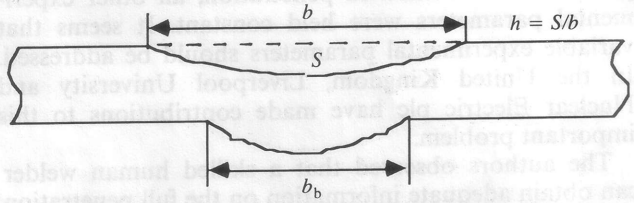

Fig. 2 Cross-section of a full-penetration weld

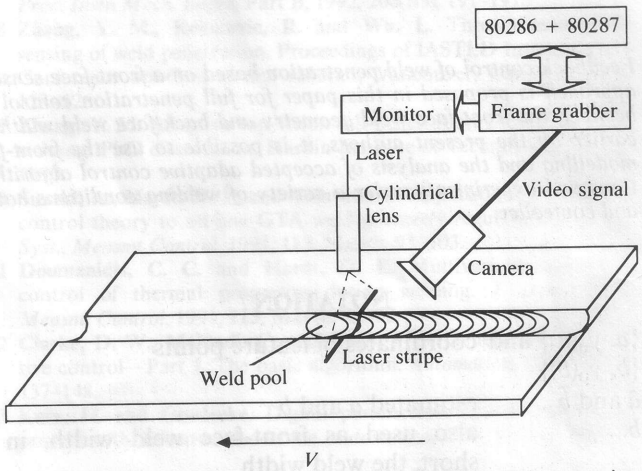

Fig. 3 Structured-light three-dimensional vision-sensing principle

been included in this laser stripe which can be acquired by processing the weld-stripe image on the xy image plane. (On this plane, the x-axis and the y-axis correspond to the transverse and vertical directions of the weldment, respectively.) The technical data of this sensor can be found in reference (**18**).

In order to depress the image noise caused by the arc light and the radiation from the hot metal, a narrow-band filter is employed. The weld-stripe image is acquired by the camera and is then converted into a digital grey-scale matrix by means of a real-time frame grabber.

Although the narrow-band optical filter can eliminate most energy of the arc light and the hot radiation, serious noise will still be caused by the arc light and the hot radiation if the stripe is too close to the pool. However, the distance between the rear boundary of the pool and the laser stripe cannot be too large owing to the problem of control delay. The distance between the electrode and the laser stripe was chosen to be 20 mm (about 5 mm behind the pool boundary). The resolutions of this sensor are $pixel_x = 0.05$ mm along the x-axis and $pixel_y = 0.0436$ mm along the y-axis, respectively.

2.2 Real-time processing of weld-stripe images

Figure 4 shows a typical weld-stripe image. In general, the following five steps are required to acquire the weld

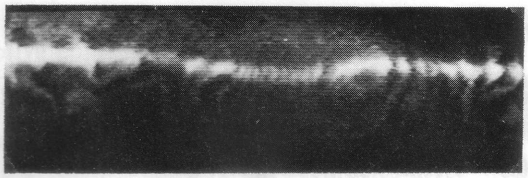

Fig. 4 Typical weld-stripe image

geometric parameters from the weld-stripe images:

(a) image filtering or noise suppression;
(b) a grey-level to binary image conversion;
(c) medial axis of the laser stripe extraction, that is laser stripe thinning;
(d) feature points of the medial axis recognition;
(e) weld geometric parameters computation based on the medial axis and the feature points.

The above procedures are time consuming. For the sake of real-time control of GTAW, a processing time of less than 0.25 s is required. Thus, an image-processing technique is proposed based on the image characteristics following

(a) adaptive dynamic medial axis extraction;
(b) unbiased feature points recognition;
(c) weld geometric parameters computation.

The medial axis extraction is discussed first.

To solve the conflict between the computational speed and the window size, a dynamic thinning procedure (DTP) is proposed based on the assumption that the laser stripe is continuous. The essence of this procedure is to begin the search along the y-axis for the maximum grey-scale point from an initial point which is close to the maximum grey-scale point. The set of points along the x-axis originating from this maximum scale point is selected to be the medial axis of the laser stripe. According to the assumption on the continuity, the vertical coordinate of this initial point can be assumed to be the vertical coordinate of the neighbouring maximum grey-scale point, which is readily available. Thus, if the assumption on the continuity of the laser stripe is true, no more maximum grey-scale points are located along the y-axis over a large range except the first one found in each frame image. The computational time will be significantly reduced.

When the laser stripe is continuous, the aforementioned DTP always functions properly. However, during actual welding, the continuity of the laser stripe cannot be guaranteed. In this case, the DTP will not work properly. In order to overcome the influence of the discontinuity on the thinning, a modified dynamic thinning algorithm, namely the adaptive dynamic thinning algorithm (ADTA), is proposed.

The adaptive dynamic thinning algorithm first determines if $\{x, y_0^*(x)\}$ (which is selected by the DTP) is on the laser stripe. If $y_0^*(x)$ is regarded to be on the laser stripe, $\{x, y_0^*(x)\}$ is accepted as a point of the laser stripe, and is denoted by $\{x, y_0(x)\}$. Otherwise, the search for $\{x, y_0(x)\}$ is extended to a larger range along the y-axis.

Experiments reveal the ADTA to be robust to the various disturbances encountered during actual welding. Examinations show that the computational time is guaranteed to be less than 80 ms on the experimental set-up.

The medial axis consists of three segments: two straight lines and a curve. The curve corresponds to the weld depression and the two straight lines correspond to the sides of the weldment. These three segments are divided by two points $\{a, y_0(a)\}$ and $\{b, y_0(b)\}$ (see Fig. 5), called the feature points of the medial axis. In order to compute the weld geometric parameters accurately, the feature points must be recognized unbiasedly. However, owing to the disturbances from the arc light and the radiation of weldpool, it is very difficult to obtain an ideal medial axis. Furthermore, in many cases, the feature points may not be apparent, since the degree of the weld depression is small.

Assume a medial axis as shown in Fig. 5. The intention is to determine the horizontal coordinates of the feature points $\{a, y_0(a)\}$ and $\{b, y_0(b)\}$, (that is a and b). In the following discussion, only a is considered, since b can be recognized in the same manner.

Suppose the equation of the straight line on the left-hand side of a is

$$y_0 = k_0 + k_1 x + \varepsilon_x, \qquad x \leqslant a \tag{1}$$

The curve on the right-hand side of a in the vicinity of a can be approximated by a linear equation:

$$y_0 = d_0 + d_1 x + \varepsilon_x, \quad x > a \tag{2}$$

where $\varepsilon_x \sim N(0, \sigma^2)$ is the Gaussian white noise representing the error of the medial axis extraction.

Suppose $\hat{a}$ is the horizontal coordinate of a point on the medial axis on the left-hand side of a ($\hat{a} \leqslant a$). We estimate (k_0, k_1) and (d_0, d_1) by the least-squares method based on the point sets $\{\hat{a} - j, y_0(\hat{a} - j)\}(j = 1, 2, \ldots, M)$ and $\{(\hat{a} + j, y_0(\hat{a} + j)\}(j = 1, 2, \ldots, M)$, respectively. The corresponding least-squares estimates are denoted by $\{\hat{k}_0(\hat{a}), \hat{k}_1(\hat{a})\}^T$ and $\{\hat{d}_0(\hat{a}), \hat{d}_1(\hat{a})\}^T$.

According to the maximum principle of the slope difference (**19**), the following $\hat{a}$ is an unbiased estimate of a:

$$\hat{a}: \max_{\hat{a} \in (a-M,\, a+M)} \{\hat{d}_1(\hat{a}) - \hat{k}_1(\hat{a})\} \tag{3}$$

Thus, an unbiased recognition algorithm for feature points can be obtained. The resulting algorithm costs about 12 ms. The identified feature points of the typical image in Fig. 4 are illustrated in Fig. 6.

The three parts of the medial axis are then fitted to a linear, a quadratic, and a linear model utilizing the least-squares method, respectively, progressing from left to right on the image. Suppose the resulting models are $l_1(x)(x \leqslant a)$, $c_2(x, x^2)(a < x < b)$ and $l_3(x)(x \geqslant b)$, respectively. The point intersected by l_1 and c_2 is (a^*, y_1^*); the intersection point of c_2 and l_3 is (b^*, y_2^*). Denote the straight line connecting (a^*, y_1^*) and (b^*, y_2^*) as l_2. Then we can employ the following equations to compute the

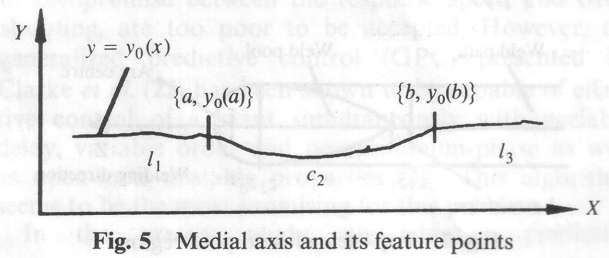

Fig. 5 Medial axis and its feature points

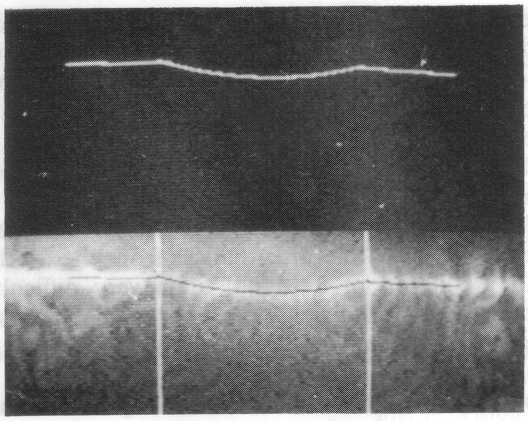

Fig. 6 Processing of typical image

weld geometric parameters of interest:

$$\text{weld width} = b^* - a^* \tag{4}$$

$$\text{average depression depth} = \frac{\int_{a^*}^{b^*} (l_2 - c_2)\mathrm{d}x}{(b^* - a^*)} \tag{5}$$

Experiments have shown that the image-processing algorithm proposed in this section always functions well during actual welding. The total time for the image sampling, the image processing and the weld geometric computation is less than 200 ms on the experimental set-up. Thus, it is regarded as a real-time algorithm.

3 MODELLING

For robotic welding, the torch speed is preprogrammed. The welding current and arc length can be more conveniently adjusted on-line. Thus, the welding current i and arc length l are selected to adjust the front-face geometry in our closed-loop control system to overcome the influence of the variations in welding conditions, with a constant predetermined torch speed.

Suppose the view shown in Fig. 7 is obtained at the kth sampling instant. At this instant, the laser stripe lies at z_3. Define

1. The weld width and depression at z_3 by $b(k)$ and $h(k)$, respectively
2. The welding current and arc length at this instant, corresponding to the arc positioned at z_0, by $i(k)$ and $l(k)$

3. $d_1 = \dfrac{z_1 - z_3}{TV}$

4. $M_1 = \dfrac{z_0 - z_1}{TV}$

5. $d_2 = \dfrac{z_2 - z_3}{TV}$

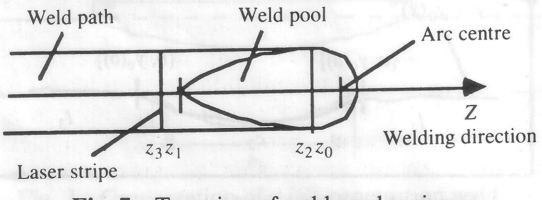

Fig. 7 Top-view of weld pool region

6. $M_2 = \dfrac{z_0 - z_2}{TV}$

where T is the sampling period and V is the torch velocity. Thus, the following model can be obtained:

$$\begin{cases} h(k) = f_1[i(k - M_1 - d_1), \ldots, i(k - d_1), \\ \qquad l(k - M_1 - d_1), \ldots, l(k - d_1)] \\ b(k) = f_2[i(k - M_2 - d_2), \ldots, i(k - d_2), \\ \qquad l(k - M_2 - d_2), \ldots, l(k - d_2)] \end{cases} \tag{6}$$

where f_1 and f_2 are functional denotation.

It can be seen that d_1 and d_2 basically correspond to the delays of depression and weld width to the arc, respectively. Similarly, M_1 and M_2 essentially correspond to the effect intervals of arc on the depression and the weld width, respectively. Because both the arc length and welding current are implied by the arc, the delay caused by the arc length will, in general, be distinct from the delay owing to the welding current. Similarly, the effect intervals of arc length and of welding current are also different. Thus, we define d_{11} as the delay of h to i, d_{12} as the delay of h to l, d_{21} as the delay of b to i, d_{22} as the delay of b to l, M_{11} as the effect interval of i to h, M_{12} as the effect interval of l to h, M_{21} as the effect interval of i to b, M_{22} as the effect interval of l to b. Using these definitions, the following equations can be generated:

$$\begin{cases} h(k) = f_1[i(k - M_{11} - d_{11}), \ldots, i(k - d_{11}), \\ \qquad l(k - M_{12} - d_{12}), \ldots, l(k - d_{12})] \\ b(k) = f_2[i(k - M_{21} - d_{21}), \ldots, i(k - d_{21}), \\ \qquad l(k - M_{22} - d_{22}), \ldots, l(k - d_{22})] \end{cases} \tag{7}$$

In equation (7), M_{ij} and $d_{ij} (i = 1, 2; j = 1, 2)$ are the sub-order and the sub-delay of the system, respectively. Since the distances from z_1 to z_0 and z_2 to z_0 are affected by the weldpool size, d_{ij} and M_{ij} are inflenced by the weldpool size as well. This produces uncertainty in the order and delay of the model.

It is well known that the weld width varies linearly with the welding current. Also, a linear model can be employed to describe the relationship between the back-face width and the welding current for full penetration GTAW (**20**, **21**). Thus, a linear relationship between the depression and the welding current can be assumed because of the linear relationship between the back-face width b_b and the depression h (**16**). Regarding the effect of the arc length on weld parameters, linear relationships have been suggested by our experiments. Thus, the following moving-average (MA) model is considered:

$$\begin{cases} h(k) = b_{10} + \sum_{j=1}^{M_{11}} b_{11}(j) i(k - j - d_{11}) \\ \qquad + \sum_{j=1}^{M_{12}} b_{12}(j) l(k - j - d_{12}) + \varepsilon_1(k) \\ b(k) = b_{20} + \sum_{j=1}^{M_{21}} b_{21}(j) i(k - j - d_{21}) \\ \qquad + \sum_{j=1}^{M_{22}} b_{22}(j) l(k - j - d_{22}) + \varepsilon_2(k) \end{cases} \tag{8}$$

where $\varepsilon_1(k)$ and $\varepsilon_2(k)$ are independent white-noise sequences. Note that, from the standpoint of decreasing

the number of parameters for on-line estimation in adaptive control, a model with an autoregression term is preferred (**22**). However, it has been found that the k-step-ahead accuracy of ARMA models decreases significantly with k. In the range of interest for our long range predictive control, the accuracies associated with the above MA models are much better than the ARMA models. Thus MA models are selected.

Experiments under six typical welding conditions are considered. For each piece of experimental data, an individual mathematical model can be obtained. For all the experimental data, a general model can be acquired to describe the general characteristics of the process. From this general model, the control algorithm will be designed. From the six individual models the performance of the designed algorithm, in overcoming the practical disturbances, will be investigated through simulation. The details of these typical conditions can be seen in reference (**17**).

All the weldments are type 321 austenitic strainless steel (18Cr 9Ni Ti) and have dimension of 100 mm in width, 250 mm in length, and 3 mm in thickness. The electrode is 2 percent thoriated tungsten 3 mm in diameter. The torch velocity is 2 mm/s, and the sampling period is 0.5 s. High purity argon gas is employed as the shielding gas. Details of the experiments have already been discussed (**17**).

The least-squares method and the F-test ($\alpha = 0.05$) are employed to identify the individual models. In order to obtain the general model, $h'(k) = h(k) - b_{10}$ and $b'(k) = b(k) - b_{20}$ are first calculated using corresponding individual b_{10} and b_{20}. Then $h'(k)$ and $b'(k)$ of all the six experiments are employed to identify a unique model. The resulting general model is

$$\begin{aligned}
h'(k) = &-0.3845l(k-16-1) + 0.0364 \\
&\times i(k-9-1) + 0.0107i(k-9-2) \\
&+ 0.0214i(k-9-3) + 0.0064 \\
&\times i(k-9-4) + 0.0075i(k-9-5) \\
&+ 0.0318i(k-9-6) + 0.0240 \\
&\times i(k-9-7) + 0.0406i(k-9-8) \\
&+ 0.0149i(k-9-9) + 0.0120 \\
&\times i(k-9-10) + 0.0221i(k-9-11) \\
&+ 0.0175i(k-9-12) + 0.0377 \\
&\times i(k-9-13) + \varepsilon_1(k) \triangleq g_1(i, l, k) + \varepsilon_1(k) \\
b'(k) = &\ 4.17l(k-17) + 0.3648i(k-15-1) \\
&+ 0.1819i(k-15-2) \\
&+ 0.1600i(k-15-3) + 0.1632 \\
&\times i(k-15-4) + 0.0564i(k-15-5) \\
&+ 0.2155i(k-15-6) + \varepsilon_2(k) \\
&\triangleq g_2(i, l, k) + \varepsilon_2(k) \qquad (9)
\end{aligned}$$

where both g_1 and g_2 are the deterministic functions of the current, arc length and discrete time, and the variances of ε_1 and ε_2 are 1.200^2 $pixel_y^2$ and 9.193^2 $pixel_x^2$, respectively.

Since practical disturbances of welding conditions are difficult to measure, the best *a priori* description of characteristics of the process is given by the general model as shown in equation (9). As the welding process proceeds, the influences of disturbances of welding conditions on the welding process will become apparent. Thus, the model can be modified based on the observation of the process. It is important, therefore, to obtain a better modified model from the initial *a priori* model. However, in this case, the number of parameters in the MA model is large and the duration of the process is short (only 200 sampling instants). Therefore, only a few key parameters can be identified on-line. Thus, the following model can be proposed using the description of $g_j (j = 1, 2)$:

$$\begin{cases} h(k) = b_{10} + \lambda_1 g_1(i, l, k) \\ b(k) = b_{20} + \lambda_2 g_2(i, l, k) \end{cases} \qquad (10)$$

where λ_1 and λ_2 are the gain modification coefficients, and b_{10} and b_{20} are the base values. During welding, λ_j and b_{j0} $(j = 1, 2)$ will be identified on-line. By adaption of the gain modification coefficients and base values, this real-time model better incorporates the general characteristic (described by g_1 and g_2) to h, b which are encountered during actual welding.

The effectiveness of the real-time model should be verified through the control performance. It has been shown by the simulations of predictive control, where the six typical welding conditions are emulated by the individual models and the real-time model is utilized by the controller, that the proposed real-time model is sufficient for this problem (**19**). In Section 5, this effectiveness will be further demonstrated through the experiments.

4 ADAPTIVE CONTROL

It can be shown that the controlled process is a non-minimum phase plant with high and variable model orders, large and variable delays and variable model parameters. Owing to the short welding duration, only a few key parameters can be identified on-line instead of all the model parameters, orders and delays. Consequently, inexact orders and delays must be addressed. Thus, conventional adaptive algorithms such as the generalized minimum variances (GMV) or pole-placement will probably fail if applied to our problem. For example (**22**), the GMV performs poorly if the plant delay varies, even if it is robust with respect to the assumed model order. Other approaches (**23**), which attempt to estimate the delays using operating data, tend to be complex and lack robustness. Unless special precautions are taken (**22**), pole-placement and the LQG self-tuners are sensitive to the overestimation of the model order owing to the pole-zero cancellations in the identified model. Also, the possibility of applying a multivariable PID or fuzzy controller has been investigated through simulations. Their performances, in terms of compromise between the response speed and overshooting, are too poor to be accepted. However, the generalized predictive control (GPC) presented by Clarke *et al.* (**22**) has been shown to be capable of effective control of a plant simultaneously with variable delay, variable order and non-minimum-phase as well as open-loop unstable properties (**22**). This algorithm seems to be the most promising for this problem.

In the present study, an adaptive predictive

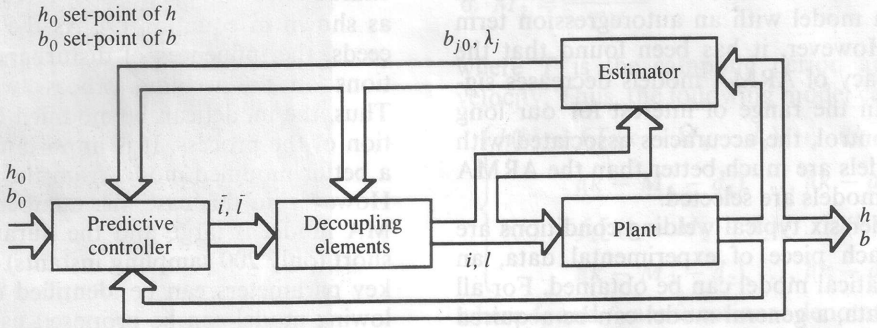

Fig. 8 Adaptive decoupling predictive control of full penetration

decoupling control scheme, utilizing GPC as the essential control strategy, is proposed. Its principle is shown in Fig. 8. The control system consists of four essential parts namely, the plant, the estimator, the predictive control algorithms, and the decoupling elements. In Fig. 8, the plant is the full penetration process (FPP) with the welding current and arc length as inputs and the depression and weld width as outputs. The estimator identifies on-line the key parameters in the real-time model which include the base values b_{j0} and the gain modification coefficients λ_j $(j = 1, 2)$, based on the input/output data, and feeds the identified results to predictive control algorithms and the decoupling elements. On basis of the modified model knowledge (that is the identified b_{j0} and λ_j) and the set-points of the plant, the predictive control algorithms calculate the generalized welding current $\bar{i}$ and the generalized arc length $\bar{l}$, which are inputs of the decoupling elements. Finally, in Fig. 8, the decoupling elements compute the welding current i and the arc length l, which are actual inputs of the plant, based on the modified model knowledge and both the generalized welding current $\bar{i}$ and the generalized arc length $\bar{l}$. The details of predictive control and decoupling algorithms are omitted here.

Simulation has been performed under typical welding conditions which are emulated by the individual models. It is understood from modelling that there are obvious variations within each individual model in orders, delays and model parameters. Also, the design of the control algorithm is based on the general model, which differs from each individual model. Despite these differences or variations, excellent simulation performance has been achieved. This shows that the designed control scheme is robust to all possible types of model mismatching, including order, delay and the model parameters.

5 EXPERIMENTS

Figure 9 shows a schematic diagram of the experimental system. In this system, the manipulator, which carries the torch and the camera, is driven by three step motors. These step motors are controlled by the computer through corresponding interfaces. Thus, the computer can adjust the arc length on-line. Also, there is a closed-loop controller of the welding current in the welder. The current can be controlled by the computer through the D/A converter.

Extensive experiments have been conducted to verify the effectiveness of the designed system. The torch velocity, sampling period, and workpiece material and size are the same as in modelling experiments. The angle θ of the electrode tip varies in different experiments. These experiments have shown that the proposed system functions well under a range of variations in welding conditions. In this paper, the experiment under varying heat-transfer condition is discussed as an example. In this experiment, $\theta = 60°$.

The varying heat-transfer condition is emulated by the geometry of the testpiece (see Fig. 10c and Fig. 11c). The bead-on-plate is performed. The rate of argon flow is 10 litre/min. The closed-loop and open-loop results are shown in Figs 10 and 11, respectively.

Because of the distance between the electrode and the laser stripe (20 mm), the weld path begins at $t = 10$ s in Fig. 10a. Also, in the first 24 s, the control algorithm is

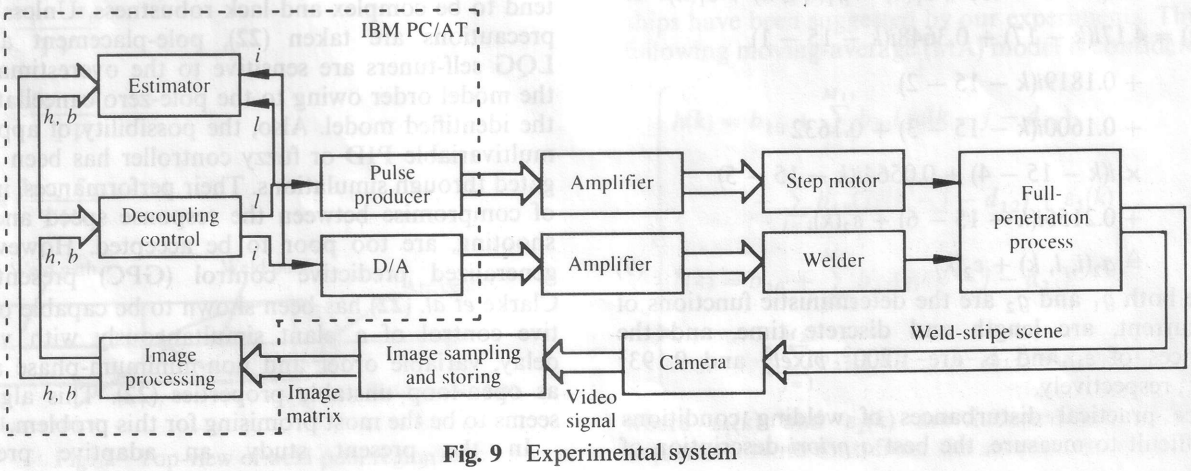

Fig. 9 Experimental system

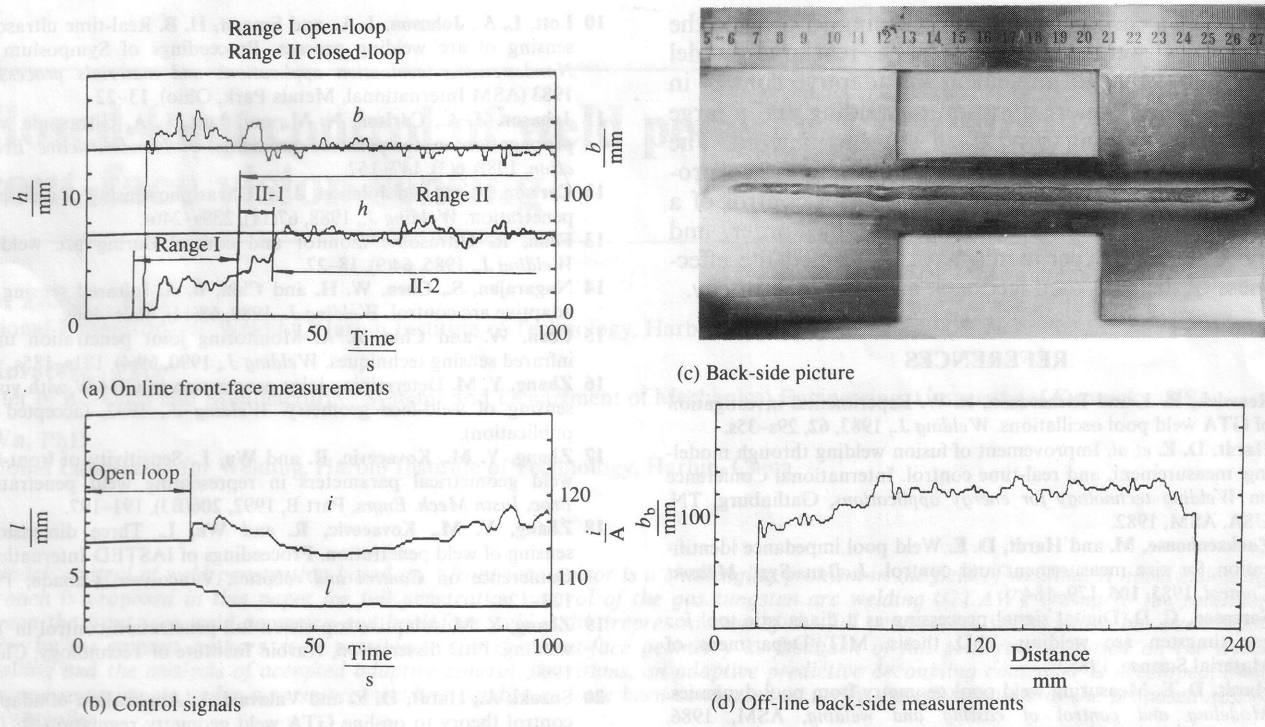

Fig. 10 Closed-loop control experiment under varying heat transfer condition

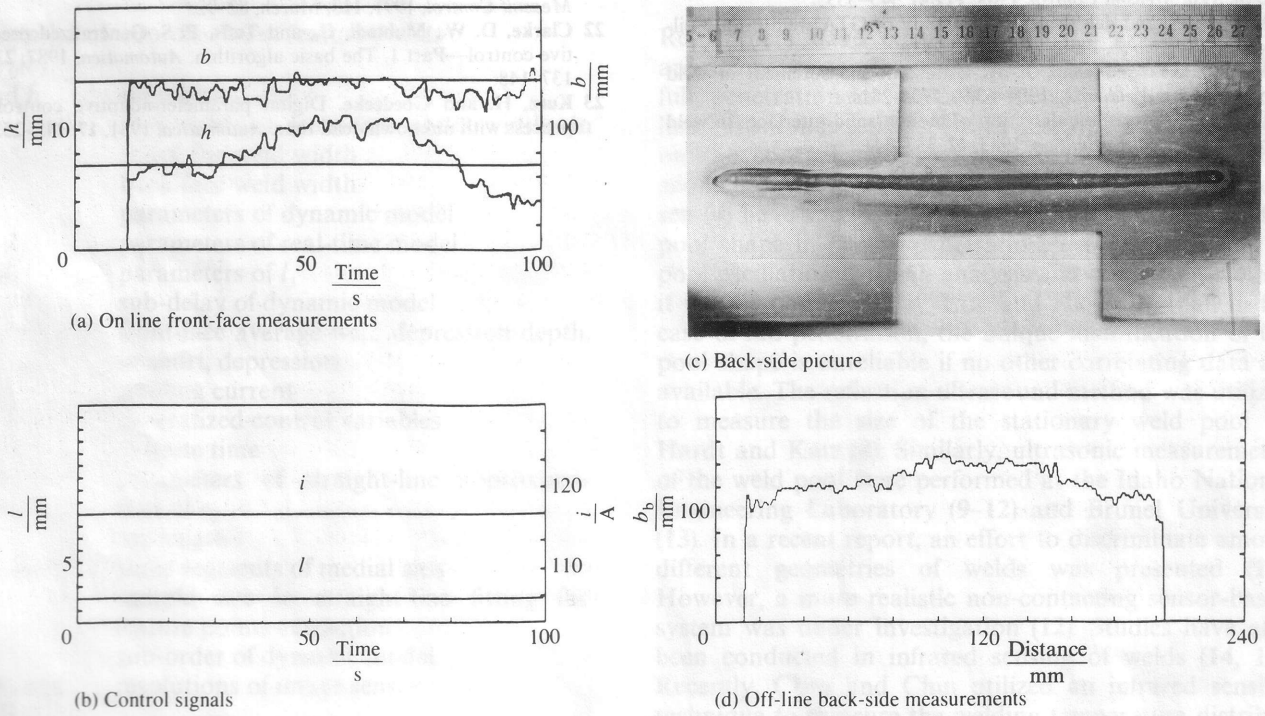

Fig. 11 Open-loop control experiment under varying heat transfer condition

open-looped. This corresponds to the range I. After this range, the closed-loop algorithm works. The range II-1 in Fig. 10a is the transient period. Although the initial weld parameters are poorly selected, the required values of geometrical parameters are also acquired by the closed-loop controller in this short period without overshooting. Then the weld geometrical parameters are well maintained despite the serious variation of heat-transfer condition (range II-2). On the other hand, for the open-loop control, the poor performance has been generated, although the welding parameters have been well selected. These show that the performance of the designed system and the control algorithm associated with the real-time model are acceptable.

6 CONCLUSIONS

A novel approach has been proposed for real-time feedback and control of weld penetration. The three-dimensional geometry of the adjacent weld behind the

pool is first measured during arc welding to provide the feedback of weld penetration. The real-time model makes it possible to implement an adaptive control in the case where a short duration of welding and a large variation in welding conditions are encountered. The adaptive decoupling predictive control algorithm provides a robust solution to the problem of control of a non-minimum-phase plant with variable order and delay. Extensive experiments have confirmed the effectiveness of the proposed feedback and control strategy.

REFERENCES

1 **Renwick, R. J.** and **Richardson, R. W.** Experimental investigation of GTA weld pool oscillations. *Welding J.*, 1983, **62**, 29s–35s.

2 **Hardt, D. E.** *et al.* Improvement of fusion welding through modeling, measurement, and real-time control. International Conference on *Welding technology for energy applications*, Gatlinburg, TN, USA, ASM, 1982.

3 **Zacksenhouse, M.** and **Hardt, D. E.** Weld pool impedance identification for size measurement and control. *J. Dyn. Syst. Measmt Control*, 1983, **105**, 179–184.

4 **Sorensen, C. D.** Digital signal processing as a diagnostic tool for gas tungsten arc welding. PhD thesis, MIT Department of Material Science, 1985.

5 **Hardt, D. E.** Measuring weld pool geometry from pool dynamics. *Modeling and control of casting and welding*, ASM, 1986. (American Society of Metals).

6 **Tam, A. S.** and **Hardt, D. E.** Weld pool impedance for pool geometry measurement: stationary and nonstationary pools. *J. Dyn. Syst. Measmt Control*, 1989, **111**(4), 545–553.

7 **Xiao, Y. H.** and **den Ouden, G.** A study of GTA weld pool oscillation. *Welding J.*, 1990, **69**(8), 289s–293s.

8 **Hardt, D. E.** and **Katz, J. M.** Ultrasonic measurement of weld penetration. *Welding J.*, 1984, **63**(9), 273s–281s.

9 **Lott, L. A.** Ultrasonic detection of molten/solid interfaces in weld pools. *Material Evaluation*, 1983, **42**, 337–341.

10 **Lott, L. A., Johnson, J. A.,** and **Smartt, H. B.** Real-time ultrasonic sensing of arc welding process. Proceedings of Symposium on *Nondestructive evaluation applications and materials processing*, 1983 (ASM International, Metals Park, Ohio), 13–22

11 **Johnson, J. A., Carlson, N. M.,** and **Lott, L. A.** Ultrasonic wave propagation in temperature gradients. *J. Nondestructive Evaluation*, 1988, **6**(3), 147–157.

12 **Carlson, N. M.** and **Johnson, J. A.** Ultrasonic sensing of weld pool penetration. *Welding J.*, 1988, **67**(11), 239s–246s.

13 **Fenn, R.** Ultrasonic monitor and control during arc welding. *Welding J.*, 1985, **64**(9), 18–22.

14 **Nagarajan, S., Chen, W. H.** and **Chin, B. A.** Infrared sensing for adaptive arc control. *Welding J.*, 1989, **68**(11), 462s–466s.

15 **Chen, W.** and **Chin, B. A.** Monitoring joint penetration using infrared sensing techniques. *Welding J.*, 1990, **69**(4), 181s–185s.

16 **Zhang, Y. M.** Determining joint penetration in GTAW with vision sensing of weld-face geometry. *Welding J.*, 1992, (accepted for publication).

17 **Zhang, Y. M., Kovacevic, R.** and **Wu, L.** Sensitivity of front-face weld geometrical parameters in representing weld penetration. *Proc. Instn Mech. Engrs*, Part B, 1992, **206**(B3), 191–197.

18 **Zhang, Y. M., Kovacevic, R.** and **Wu, L.** Three dimensional sensing of weld penetration. Proceedings of IASTED International Conference on *Control and robotics*, Vancouver, Canada, 1992, 123–126.

19 **Zhang, Y. M.** Adaptive top-vision full penetration control in TIG welding. PhD dissertation, Harbin Institute of Technology, China, 1990.

20 **Suzuki, A., Hardt, D. E.** and **Valavani, L.** Application of adaptive control theory to on-line GTA weld geometry regulation. *J. Dyn. Syst., Measmt Control*, 1991, **113**, March, 93–103.

21 **Doumanidis, C. C.** and **Hardt, D. E.** Multivariable adaptive control of thermal properties during welding. *J. Dyn. Syst., Measmt Control*, 1991, **113**, March, 82–92.

22 **Clarke, D. W., Mohtadi, C.,** and **Tuffs, P. S.** Generalized predictive control—Part 1. The basic algorithm. *Automatica*, 1987, **23**(2), 137–148.

23 **Kurz, H.** and **Goedecke.** Digital parameter-adaptive control of process with unknown dead time. *Automatica*, 1981, **17**, 245–252.